Raney-Platinum thin film electrodes for the catalysis of glucose in abiotically catalyzed micro glucose fuel cells

Uyen P. Do [1] , iD: <u>0000-0002-8283-5612</u>, <u>phuong.uyen.do@gmail.com</u>
Frode Seland [2] , iD: 0000-0002-2901-8314, <u>frode.seland@ntnu.no</u>
Kaiying Wang [1] , iD: <u>0000-0002-0018-0959</u>, <u>Kaiying.Wang@usn.no</u>
Erik A. Johannessen [1,*] , iD: <u>0000-0002-2222-8140</u> , <u>eaj@usn.no</u>

[1] Department of Microsystems, Faculty of Technology, Natural and Maritime Sciences, University of South-Eastern Norway Raveien 215, 3184 Borre, Norway
[2] Department of Materials Science and Engineering, Faculty of Natural Sciences and Technology, Norwegian University of Science and Technology, NTNU 7491 Trondheim, Norway
* Corresponding author: E.A Johannessen, Tel.: +47 31 00 93 85, <u>eaj@usn.no</u>

<u>Abstract</u>

Fuel cells capabable of synthetic glucose catalysis have revolved around the implementation of abiotic catalysts that require extreme acid and alkaline environments. These are not compatible with implantable medical sensor systems, and hence there is a need to develop abiotic catalysts that operate at neutral pH. This paper presents structural and electrochemical characteristics of a nanoporous electrode designed for abiotic glucose oxidation in the presence of oxygen in neutral physiological media. The electrode was fabricated by annealing e-beam deposited thin films of Platinum (Pt) and Nickel (Ni) into a Pt-Ni alloy on a silicon substrate. The porous nature of the alloy enhance electrochemical properties by increasing the real surface area ~ 500 times compared to the geometric surface area of as-prepared multilayer thin films. This was reflected in the exchange current density of the electrode annealed at 800 $°C$ being twice that of the electrode annealed at 650 $°C$. The cell voltage increase, due to the addition of dissolved physiological oxygen of 2 ppm, was about 100 ± 8 mV under a load current density of 2 $\mu A\ cm^{-2}$. After running for 72 hours in a physiological saline solution with 5 mM glucose, the increase in the electrode potential was only 23 $\mu V\ h^{-1}$. These results suggest that the nanoporous Pt-Ni alloy anode offers an improved catalytic stability with time and should be a viable candidate for use in abiotic catalysed glucose fuel cell systems operating under physiological conditions.

1 Introduction

Implantable electronic devices have successfully been used in biomedical applications since the invention of the artificial pacemaker more than five decades ago [1]. The concept of miniaturised electronic systems have since been promoted to various clinical activities [2] such as, implantable neuroprosthetic devices [3], immuno-isolation barriers [4], drug delivery [5], microinjection [6], pH detection [7] and blood pressure monitoring systems [8],[9]. Although batteries have been considered as the first choice as a driven power supply, they suffer from the size constraints of the implant combined with a relatively low energy storage capacity. This combination will limit the operational lifetime of the device, and hence there is an interest to develop alternative power supply systems that does not require recharging or replacement. A group of promising candidates revolves around scavenger devices that harvest energy from thermal gradients [10, 11], vibration [12, 13] or exogeneous chemicals [14, 15]. The latter offers the greatest energy density of these three schemes, from which the glucose fuel cell (FC) may be the most viable alternative. Glucose FCs generate electric current from the oxidation of glucose and the reduction of dissolved oxygen (DO). Both glucose and DO are found in abundance throughout the body, and a power harvesting regime based on these exogeneous fuels offers the promise of a potential long-term power supply for miniaturised electronic medical implants.

Glucose FCs can be divided into three main types according to the catalyst used to facilitate the electrode reactions: (i) Enzymatic, which use immobilised enzymes such as glucose oxidase or hexokinase in their isolated forms to speed up the catalysis of glucose and therfore the current output [16, 17]; (ii) Microbial, which utilize the whole enzymatic system of microorganism such as yeast and bacteria to fully oxidize glucose to its end products CO_2 and water [18]; and (iii) Abiotical, which make use of non-biological materials, such as noble metals and their alloys as well as activated carbon, to catalyse the electrochemical reactions [19],[20]. The power densities of the latter are lower than the other two types, but they benefit from extended operational lifetimes and a higher stability by not relying on biological agents that degrades with time. Although a microbe population may regenerate, microbial fuel cells are not seriously considered for implantation due to the infective nature of most known micro-organisms and the associated risks therewith [21].

The first tests of glucose oxidation based on abiotic electrode-catalysts was published back in 1964 [22], and literature have since reported the use of different electro-catalytic materials tailored spesific electrolytes. Platinum (Pt) have in general been found to be a universally good catalyst of glucose especially in acidic media [23], whereas palladium exhibits best performance in neutral and alkaline media [24, 25]. Unfortunately, these pure metal electrodes have a tendency of losing their activity with time due to "poisoning" [23] or the inactivation due to partial oxidation of glucose leading to formation of strongly bound carbon monoxide, CO(ads), blocking the active surface sites [26]. Raney-Pt alloys, made of Pt and a non-noble metal such as Zinc (Zn), Lead (Pb), Nickel (Ni) or Aluminum (Al) [27-30] are also promising candidates for abiotic catalysis due to their lower cost of production, good catalytic activity towards glucose and low sensitivity to DO. The latter is an important parameter given that glucose and DO exist in the same solution. However, their performance as thin film electrodes has yet to be explored.

This paper presents a comprehensive analysis of the catalytic activity of electrodes made from thin film Raney-Pt alloys (based on Pt and Ni) with respect to the oxidation of glucose. These metal films were deposited by e-beam evaporation (with sputtering and thermal deposition methods being optional alternatives). The thicknesses of thin films range from a few nm and up

to one micrometer [31] compared to the thicker micrometer range electrodeposited/plated films reported in literature [28]. Although the microfabrication compatibility of thin films shares a benefit of integration with miniaturised circuits and systems, these are challenged with a lower surface roughness due to the limited thickness of the metal. Hence a post processing step that results in a roughened alloy film that increases the real surface area is presented in this paper. The Pt-Ni electrodes were characterized for its glucose selective properties under simulated physiological conditions both in the presence and absence of oxygen by using cyclic voltammetry, polarization and electrochemical impedance spectroscopy. The Pt-Ni electrodes were also characterized electrochemically in order to investigate the real surface area and the glucose oxidation activity.

2 Materials and Methods

2.1 Fabrication

Single side polished silicon wafers with a crystal orientation of <100> (p-type, 525 ± 25 µm thickness) was used as the thin film electrode substrate (Si-Mat, Germany). Thin metal films of 20 nm Titanium (Ti), 100 nm Platinum (Pt) and 300 nm Nickel (Ni) was deposited by e-beam evaporation. The wafers were diced into 5×5 mm large samples using a dicing saw (DAD - 2H/6T, Disco Corp., Japan) before the samples were alloyed by annealing in a 2" barrel furnace (MSL, MTI Corp., USA) at two different temperatures (650 and 800 °C) for 2 hours. These two samples will hereafter be referred to as Pt-Ni$_{650}$ and Pt-Ni$_{800}$ electrodes, respectively. The annealing was performed in an inert atmosphere (N$_2$) with a flow rate of 2 L min^{-1} that flushed the system throughout the annealing process, (from 1 hour prior to and until the sample had returned back to room temperature). This reduced the formation of an oxide layer on the metal alloy. The unalloyed Ni and any nickel oxide that had formed due to residual oxygen present during the annealing process, was dissolved in a mixture of (1:1 volume) of 1 M sulfuric acid (H_2SO_4) and 0.39 M nitric acid (HNO_3) at 80°C for 2 hours. Copper wire was then bonded to the electrode using silver epoxy (EPO-TEK EE129-4, Epoxy Technology, Inc., US) to form an electrical connection before silicone rubber (3140 RTV Coating, Dow Corning, US) was applied to electrically insulate the connection from the aqueous test solution. Finally, any remaining Ni and nickel oxide was removed by electrochemical etching in a 1 M H_2SO_4 solution at 80 °C by cyclic voltammetry (CV). Ten potential cycles were performed in the potential region of -0.3 to 0.4 V vs a standard Ag│AgCl (4.0 M KCl) reference electrode (Thermo Scientific, US) at a scan rate of 10 mV s^{-1} using a potentiostat (Versastat 3, Princeton Instruments, US). All potentials reported in this work are initially quoted vs this reference electrode, although conversions to the reversible hydrogen electrode (RHE) has been done in some figures for comparison with literature data. A Pt wire (P/3640/89, Fisher Scientific Limited, UK) was coiled up and used as the counter electrode. Analysis of surface morphology, elemental composition and oxide levels of the Pt-Ni$_{650}$ and Pt-Ni$_{800}$ working electrodes were performed after each fabrication step with an EDS attached to a scanning electron microscope (XL30, Philips, Netherlands).

3

2.2 Surface area determination

Estimations of the electrochemical (real) surface area (ECSA or A_{real}) of the Pt-Ni electrodes were based on the charge under the hydrogen adsorption peaks obtained from cyclic voltammograms in 0.5 M H_2SO_4 solutions. This method is commonly used for Pt electrodes [32],[33],[34] and was adapted here for simplicity for comparison of the different samples used (and at the same time neglecting the effect of unalloyed nickel in the electrodes). A 0.5 M H_2SO_4 solution was prepared freshly and deaerated with N_2 purging. CVs of the electrodes were obtained at room temperature in the potential range of -0.2 to 1.2 V and at a scan rate of 50 mV s^{-1}. The charge under the hydrogen adsorption peaks was calculated in the region of -0.2 to 0.2 V. For simplicity, we assume that one hydrogen atom is being adsorbed on each active surface site and that the charge per active catalyst surface area is similar to the one for polycrystalline platinum, which is considered to be 210 μC cm^{-2} [33, 35]. The A_{real} of the Pt-Ni electrodes was then obtained by dividing the charge affiliated to the hydrogen adsorption with the charge density of a smooth polycrystalline Pt electrode.

2.3 Electrode performance

The experimental protocol is based on previous work [32], where the performance of the anode (working electrode) is monitored with respect to a separate counter and standard reference electrode (Ag|AgCl, 4.0 M KCl). The larger size of the Pt coil counter electrode and the use of a reference electrode imply that all loss terms can be assigned the anode alone. This three electrode configuration was immersed in a test solution containing 10 mM phosphate buffered saline (PBS) at pH 7,4 (P3813, Sigma-Aldrich, US). Glucose (G7525, Sigma-Aldrich, US) was added to a concentration of 5 mM in order to simulate physiological levels of the interstitial fluid in human tissue [19]. All experiments were performed at room temperature. The PBS solution with 5 mM glucose was deaerated with N_2 purging to remove dissolved oxygen (DO) in order to simulate the working condition of the Pt-Ni electrodes as a function of glucose oxidation alone. Experiments were also conducted with solutions saturated with air in order to investigate overall electrode performance in the presence of oxygen, hence possible oxygen reduction alongside glucose oxidation. The oxygen level was continuously monitored by a DO meter (C3040, Consort, Belgium). Polarization curves were obtained by applying a current step of 2 μA cm^{-2} from an initial open circuit potential (OCP) and up to 20 μA cm^{-2}, in which the electrode potential under load was recorded after 2 h when the signal had stabilised. The standard thermodynamic cell voltage (E$^o_{cell}$) for a 2-electrode cell with glucose oxidation to gluconic acid at the anode and oxygen reduction at the cathode $C_6H_{12}O_6 + \frac{1}{2}O_2 \rightarrow C_6H_{12}O_7$ is reported to be 1.30 V at standard conditions [19]. The oxidation reaction is limited to a 2 electron glucose oxidation to gluconic acid with a standard electrode potential of -0.07 V vs RHE (-0.27 vs our standard Ag|AgCl reference electrode at pH=0). The glucose oxidation is later revisited by Kerzenmacher et al. discussing various possible pathways depending on electrode materials and environment, which would also affect the true standard thermodyncamic potential of the anode [19].

In this work we are not operating at standard conditions and are merely interested in the anode performance. We measure the potential at the anode as the potential difference between the working electrode and a standard reference electrode by controlling the current passing through

the counter electrode. The anode potential (E_{anode}) can be expressed as the sum of the anodic thermodynamic (reversible) potential ($E_{rev, anode}$) and the loss-terms:

$$E_{anode} = E_{rev,anode} + \eta_{act} + \eta_{conc} + \eta_{ohm} \tag{1}$$

where η_{act} and η_{conc} are the activation and concentration overpotentials, respectively and η_{ohm} is the ohmic overpotential (resistance towards electron transfer in the electrode and wire as well as the electrolyte resistance from the working electrode to the tip of the reference electrode). At low current densities, i.e. near the reversible potential, the activation overpotential dominates due to the low driving force imposed. Thus one can assume that the transport of reactants will keep up with the charge transfer reaction resulting in essentially no concentration variations and thus a negligble concentration overpotential. However, the ohmic overpotential, being linearly dependent on current density, still needs to be considered:

$$\eta_{ohm} = j \times ASR_{ohm} \tag{2}$$

where j is the current density (A cm^{-2}) and ASR_{ohm} is the area specific resistance (Ω cm^{2}). Both current and resistance are here normalized with respect to the geometric surface area.

The Tafel slopes and apparent exchange current densities were estimated through the Tafel plot of the IR-corrected potentials ($E_{corr} = E_{anode} - \eta_{ohmic}$) vs $\log_{10} j$.

2.4 Electrochemical impedance spectroscopy

The electrochemical impedance spectroscopy (EIS) was performed in deareated solutions over a frequency range from 1x10^{-2} to 8x10^{6} Hz using the EIS function of a Zahner electrochemical workstation (IM6, Zahner-elektrik GmbH, Germany). The galvanostat mode was used, which supplied the working electrode with a constant current along with a small AC perturbation with an amplitude of 10 nA (peak to peak). The electrical equivalent circuit, presented in Fig. 1, is based on a published model of glucose oxidation on a Pt and Nickel hydroxide catalyst surface in alkaline solutions. This involves an adsorption step in addition to charge transfer in parallel to a double layer capacitance (modeled as a constant phase element) in series to the ohmic resistance [36],[37].
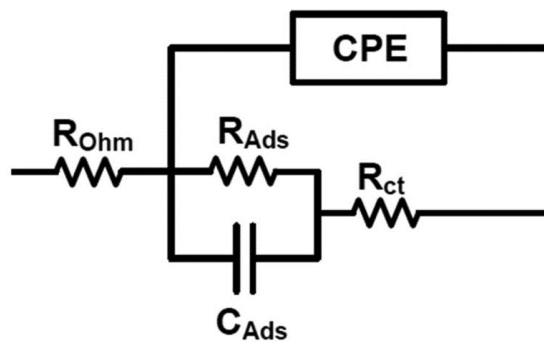
Figure 1: Electrical equivalent circuit of the Pt-Ni electrodes

This simplified model is also considered to be applicable in PBS solutions assuming a similar simplified reaction scheme [38]. The SIM function of the electrochemical workstation was used to estimate the parameters of the charge transfer resistance (R_{ct}), the ohmic resistance (R_{ohm}), the adsorption resistance (R_{ads}), the adsorption capacitance (C_{ads}) and the constant phase element (CPE) consisting of the constant representative (Q) and the exponent (m). A *CPE* is used rather than an ordinary capacitor as the added parameters (*Q, m*) satisfies the *F* ratio test for a parameter addition to the equivalent circuit [32, 39]. From the *CPE* parameters, the double layer capacitance C_{dl} is then calculated by the following equation [40]

$$C_{dl} = \left[Q \left(\frac{R_{ohm} R_{ct}}{R_{ohm} + R_{ct}} \right)^{1-m} \right]^{1/m} \tag{3}$$

3 Results and discussion

3.1 Microstructural evaluation and surface area determination

The surface topographies of the Pt-Ni electrodes, shown before and after annealing as well as (electrochemical) etching, are presented in fig. 2. Both the Pt-Ni$_{650}$ and Pt-Ni$_{800}$ electrodes exhibit comparable surface topographies, with the appearance of pin-holes which are similar to that observed for Pt film surfaces that have been annealed above 600°C [41]. The higher annealing temperature of the Pt-Ni$_{800}$ electrodes results in a topography with pin holes that are larger but distributed with a lower density compared to those generated at a lower annealing temperature of the Pt-Ni$_{650}$ electrodes. The appearance of pin holes or grooves can be linked to the induced tensile stress that appears in the Pt-Ni film as the sample cools down (due to a larger thermal expansion coefficient of the metal film compared to the silicon substrate). This will trigger Pt and Ni atoms to migrate (diffuse) along the grain boundaries towards the film-surface interface, resulting in a reduction in grain size at the film surface and subsequent hole (or thermal pit) formation [42],[43]. This trend is observed more clearly on the Pt-Ni electrodes after the unalloyed nickel and nickel oxide have been removed by chemical and electrochemical etching. The oxygen element in the EDS results (inserts of Fig 2.b and Fig 2.c) shows that there is a presence of nickel oxide on the electrode surface even though care had been taken to anneal the samples in an inert N_2 atmosphere. The removal of the unwanted nickel oxide film was confirmed by a decrease in the overall oxygen content (inserts of Fig 2.d and Fig 2. e). The removal of nickel oxide and unalloyed nickel revealed the largely rough interface of the underlying Pt-Ni alloy which increased the overall roughness of the electrode surface [44, 45].
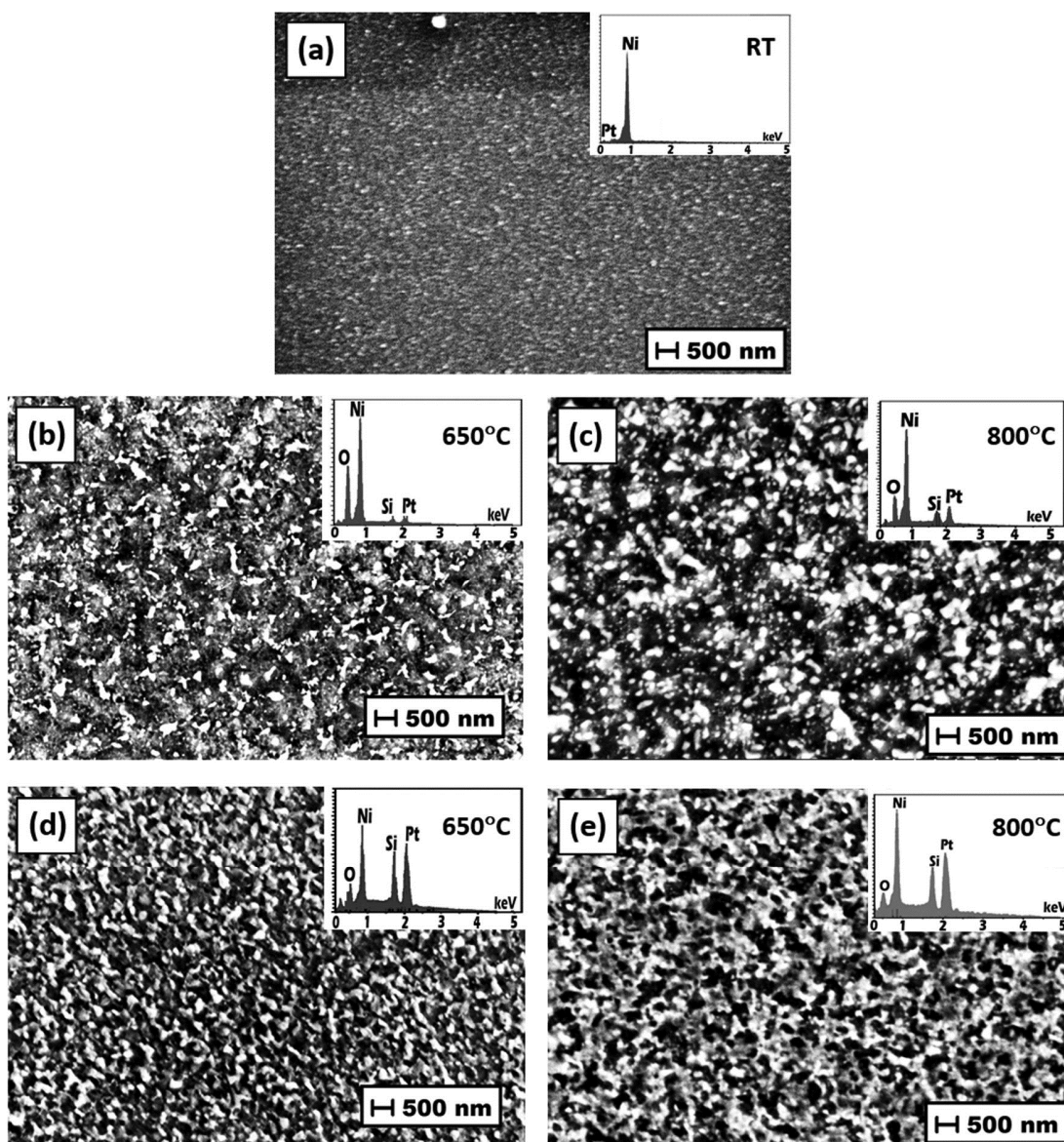
Figure 2: Surface SEM images of the Pt-Ni electrodes taken (a) before annealing and (b) after annealing at at 650° C and (c) 800° C. The same samples shown after removal of unnalloyed Ni and nickel oxide for (d) Pt-Ni$_{650}$ and (e) Pt-Ni$_{800}$ electrodes by etching. Inserts show EDS measurements for the respective electrode surfaces. RT = room temperature.

The representative CVs of the Pt-Ni electrodes conducted in 0.5 M deareated H_2SO_4 are presented in Fig 3 (the reversible hydrogen electrode (RHE) scale is shown for comparison). The Pt-Ni alloy exhibits a comparable electrochemical behavior to that of Pt in contrast to unalloyed Pt-Ni electrodes (as-prepared). The hydrogen UPD (underpotential depostion) adsorption and desorption peaks are visible below a potential of 0.3 V vs RHE (fig.3 (i)), whereas the formation of Pt oxide is visible in the potential region from 0.8 V to 1.4 V vs RHE

7

(fig.3 (iii)). The subsequent reduction of Pt oxide is seen in the negative sweep which peaks at around 0.73 V vs RHE (fig.3 (ii)). Based on the charge recorded from the hydrogen adsorption peaks, a real surface area A_{real} of 38 ± 7 and 80 ± 5 cm^2 (235 ± 44 and 492 ± 32 times larger than the geometrical surface area, A_{geo}) were obtained for the Pt-Ni$_{650}$ and Pt-Ni$_{800}$ electrodes, respectively. Although these values are smaller than that reported by Gebhardt et al. [28] for electrodes made from thicker layers of Pt and Ni (150 μm Ni on top of a 100 μm thick Pt foil) annealed at 1450° C, it is clear that the surface topography of the electrodes scales with the thickness of the material used.
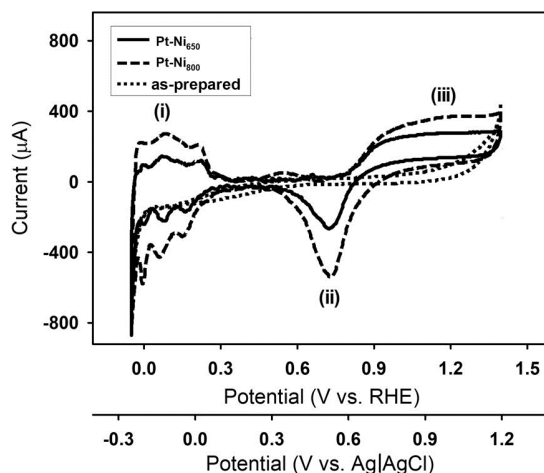

Figure 3: CV curves (10 mV s^{-1}) of alloyed Pt-Ni$_{650}$ and Pt-Ni$_{800}$ electrodes and the "as prepared" unnalloyed counterpart. The experiments were conducted in deareated 0.5 M H_2SO_4. Peak (i) corresponds to the hydrogen UPD adsorption and desorption peaks, (ii) the reduction of platinum oxide, and (iii) the formation of platinum oxide. The potential of RHE have been adjusted for 0.197 V difference from the Ag│AgCl, 4.0 M KCl. See text for details.

3.2 Electrode performance

Cyclic voltammograms of the electrodes in deareated PBS solutions with or without 5 mM glucose are shown in Fig 4 (the RHE scale is shown for comparison). Although the behavior of the Pt-Ni$_{650}$ and Pt-Ni$_{800}$ electrodes are similar to that of pure Pt electrodes through peak A, C, D and I [46-48], Ni still has its influence on the electrode behavior through peak F [49],[50, 51],[52]. Peak C in Fig. 4. is assigned to the oxide formation of Pt, whereas peak D is assigned the corresponding reduction of oxides [46-48]. In neutral solutions such as PBS, Ni could be oxidized during peak C, and then reduced, at peak F [49],[50, 52]. Peak A is assigned hydrogen desorption whereas peak I is a result of hydrogen adsorption, which is similar to that observed for pure Pt electrodes [46-48]. Since the adsorption of glucose falls within the potential range for hydrogen adsorption when the pH of the solution is in the range of pH 5.5 to 8 [38], this may occur on top of the underlying surface reactions found at peaks A and I in the hydrogen adsorption/desorption region [53]. This is further corroborated by the effective surface coverages of both glucose and hydrogen found to be at a maximum in the potential region of 0.2 - 0.22 V vs

RHE [38].

The addition of 5 mM glucose do also give rise to new oxidation peaks, such as peaks B, C and E. Since a complete oxidation of glucose to CO_2 requires the transfer of 24 electrons, this is not very likely to occur and a wide variety of possible reaction products and intermediates can be expected [19],[36],[37],[54]. Instead, the oxidation of glucose at peak B is likely to be dominated by the formation of gluconolactone which is subsequently converted to gluconic acid by hydrolysis [38],[55] i.e. a two electron process. The peak current was recorded at a potential of 0.69 and 0.75 V vs RHE for the Pt-Ni$_{650}$ and Pt-Ni$_{800}$ electrodes respectively, and falls within the region where Pt(OH) species are being formed [56]. At lower potentials the electrode is blocked by adsorbed reaction intermediates that limits the catalytic activity, but which starts to desorb at potentials higher than 0.5V vs RHE [55]. In contrast, at potentials above 0.8 V vs RHE, less active Pt oxide (Pt-O) is formed (fig.3 (iii)) which reduces the overall catalytic rate. Also, Ni beta-hydroxide can be assumed to be formed at these potentials [49],[52]. By increasing the potential beyond 1.1 V vs RHE, the oxidation of glucose seems to be somewhat reactivated around peak C. The exact reason for this is not properly understood, but a reaction takes place between glucose and the Pt-O layer [55]. In the negative (reverse) scan, negligible glucose oxidation occurs until peak E, which follows directly after the Pt oxide reduction in peak D. Peak E can therefore be attributed to the reactivation of glucose oxidation on freshly reduced Pt surface. The voltammetric features are similar to the results reported in literature with respect to pure Pt electrodes or Pt-based bimetallic electrodes, reflecting a similar glucose oxidation reaction mechanism [38, 55, 57-59].
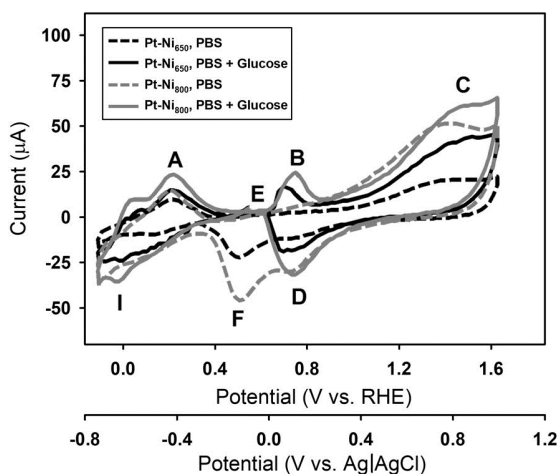

Figure 4: CV curves (10 mV s^{-1}) of the Pt-Ni$_{800}$ and Pt-Ni$_{650}$ electrodes. The experiments were conducted in deareated 10 mM PBS solutions with and without 5 mM glucose. Peak A (hydrogen desorption / glucose oxidation), B (glucose oxidation), C (platinum & nickel oxide formation / glucose oxidation), D (platinum oxide reduction), E (glucose oxidation), F (nickel oxide reduction), and I (hydrogen adsorption). The potential of RHE have been adjusted for the difference from Ag$\vert$AgCl, 4.0 M KCl at pH = 7.4 (0.197 + 0.059*pH = 0.197 + 0.437 = 0.634 V).

The polarization curves at constant currents were recorded galvanostatically for the Pt-Ni$_{650}$ and Pt-Ni$_{800}$ electrodes in 10 mM PBS with 5 mM glucose both at zero and 7 ppm DO (Fig. 5). It is worth noting the relatively low anodic potential observed for the glucose oxidation, in comparison

to the oxidation peaks B and E observed in the voltammogram (Fig. 4). It is clear that oxidation of glucose also occurs at lower overpotentials than is represented by these peaks, thus some continuous oxidation can be expected to occur in the potential region represented by peak A. In fact, we do see a small difference between the CVs with and without glucose supporting the low potentials measured in the constant current measurements. In contrast to small organic molecules like methanol, where the dehydrogenation and formation of strongly adsorbed intermediates is rather quick, glucose oxidation is governed by slow adsorption kinetics rendering the reaction as rate limited. The peak current will also be limited by adsorbed reaction intermediates blocking the surface area available for catalysis at potentials below 0.5 V vs RHE [38],[55].
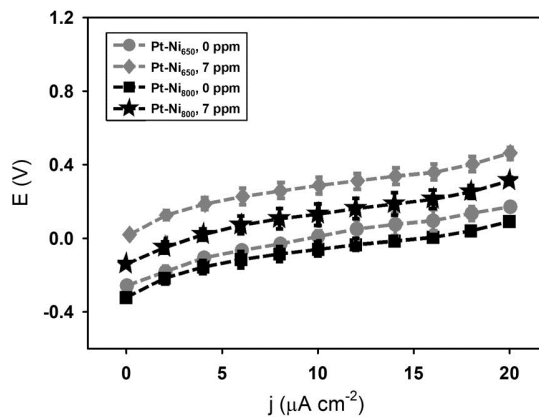

Figure 5: Individual polarization curves of the Pt-Ni$_{800}$ and Pt-Ni$_{650}$ electrodes in 10 mM PBS containing 5 mM glucose subject to zero (deareated) and 7 ppm (air saturated) DO.

The Pt-Ni$_{800}$ electrodes exhibit somewhat more negative potentials compared to the Pt-Ni$_{650}$ electrodes over the whole measurement range for each DO concentration, perhaps indicating slightly improved kinetics at the former. Interestingly, the increase in electrode potential when introducing 7 ppm DO is more severe for the Pt-Ni$_{650}$ electrode than the one treated at 800°C (Fig. 5). A comparison between the two electrodes for various DO levels at 2 µA load is shown in Fig. 6. The increase in potential of the Pt-Ni$_{650}$ and Pt-Ni$_{800}$ electrodes when DO was added into the PBS solution to a concentration of 7 ppm (Fig. 6) is approximately 127 ± 41 and 166 ± 10 mV, respectively. The potential rise at the Pt-Ni electrodes is due to a simultaneous oxygen reduction occurring when oxygen is introduced. At low electrode potentials, below the Pt oxide reduction peak (peak D in Fig. 4), one can expect that oxygen reduction occurs at its diffusion limiting current value, making the current proportional to the concentration of DO. Thus, the applied positive current must come from glucose oxidation and a higher glucose oxidation current must be drawn in order to compensate for the increased oxygen reduction current with increasing DO levels. The electrode potential follows a typical hyperbolic curve where an initial rapid increase at low DO concentrations approaches a level of saturation of the reactive sites around 7 ppm. The large change in potential (80 ± 2 and 101 ± 8 mV for the Pt-Ni$_{650}$ and Pt-Ni$_{800}$ electrodes, respectively) at low DO concentrations (typical 0 to 2 ppm in human tissue), shows that it will be preferable to design and fabricate a fuel cell system which limits oxygen availability to the anode if this is to be placed in an environment where these two components are present.

One can relate the differences in the measured potentials of the Pt-Ni electrodes in this region to the differences in the so-called effective exchange current density j_0^*:

$$j_0^* = j_0 \times \frac{A_{real}}{A_{geo}} = j_0 \times f_r \qquad (4)$$

where j_0 refers to the intrinsic exchange current density of a smooth plane surface. The ratio A_{real}/A_{geo}, is the roughness factor, f_r, representing the ratio between the real surface(A_{real}) and that of an ideally smooth plane area (A_{geo}) given by the geometric dimension of the electrode. With the roughness factors of the Pt-Ni electrodes estimated to, $f_{r650} = 235 \pm 44$ and $f_{r800} = 492 \pm 32$ respectively (section 3.1), the effective exchange current density of the Pt-Ni$_{800}$ electrodes will be about two times higher than that of the Pt-Ni$_{650}$ electrodes.
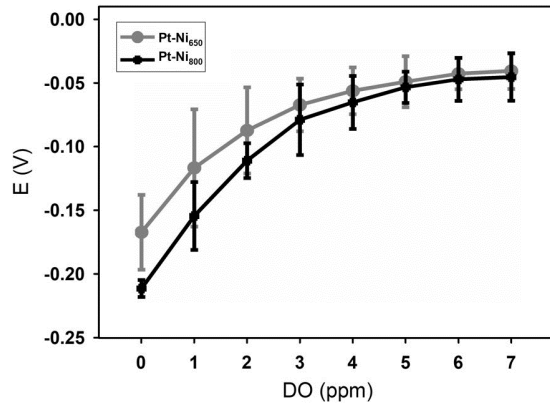

Figure 6: Chronopotentiometric response of the Pt-Ni$_{800}$ and Pt-Ni$_{650}$ electrodes in 10 mM PBS and 5 mM glucose subject to different concentrations of DO at a constant load current density of 2 $\mu A\mathrm{cm}^{-2}$

As observed with previous work on the cathode [32], so is it difficult to give a detailed consideration of the enhancement of the cell potential and exchange current density based on the roughness factor alone. However, one may tentatively suggest that an improved catalytic surface condition caused by the annealing at 800 °C could be linked to the an increase in the number of available reaction sites caused by a larger real surface area.

3.3 Electrochemical impedance spectroscopy study

The impedance of the Pt-Ni electrodes at a load current density of 2 μA cm^{-2} (as measured against the geometric surface area) are presented as Nyquist plots in Fig 7. The impedance data show two relaxations, one small at high frequencies and one larger towards lower frequencies. The appearance of a second relaxation process can be indicative of adsorption of reaction intermediates on the surface, which may be modeled as a capacitance, C_{ads}, in parallel with a resistor, R_{ads}. Consequently, an electrical circuit containing two time constants was chosen to fit

the data (Fig. 1). The same equivalent circuit was previously used to fit impedance data for Pt electrodes in PBS [37] and nickel hydroxide electrodes in alkaline solution [36]. The ohmic resistance is represented by R_{Ohm} in Fig. 1. and can be found from the high frequency intercept with the real axis. Subsequently, area-specific ohmic resistances ASR_{ohm} of the two electrodes was found to be 4.1 ± 0.7 Ω cm^2 for the Pt-Ni$_{650}$ electrode and 3.9 ± 0.8 Ω cm^2 for the Pt-Ni$_{800}$ electrode. These resistance values are low compared to the 200-250 Ω cm^2 obtained with the thin film porous palladium (Pd) electrodes developed in a previous study [32]. The constant phase element (*CPE*) describes the deviation from ideal behavior of the double-layer capacitance. The magnitude of the CPE coefficient *m* was fitted to be 0.80±0.04 and 0.76±0.06 for the Pt-Ni$_{650}$ and Pt-Ni$_{800}$ electrodes, respectively. A decrease in *m* may be interpreted as an increasing surface roughness, as the classical concept of the double layer capacitance of an ideally smooth and uniform electrode / solution interface becomes progressively less applicable [36],[60].
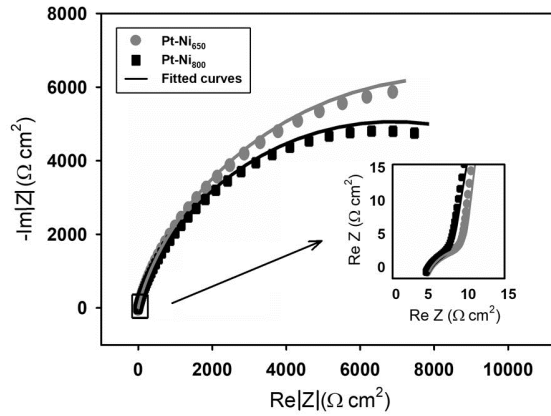

Figure 7: Nyquist plot obtained from the Pt-Ni$_{650}$ and Pt-Ni$_{800}$ electrodes at a load current density of 2 μ A cm^{-2} in deareated PBS solution with 5 mM glucose.

The relationship between the load current density and the circuit elements representing the charge transfer resistance (R_{ct}), the double layer capacitance (C_{dl}) as extracted from the constant phase element (Eq. 5), the adsorption resistance (R_{ads}), and the adsorption capacitance (C_{ads}) is presented in Fig. 8. The resistance elements R_{ct} and R_{ads}, which are related to the kinetics of the interfacial charge transfer reaction, cannot be interpreted simply as successive charge transfer resistances for individual reaction steps. They are instead attributed to the properties of two or more steps in the overall reaction [36]. The electro-oxidation of glucose is governed by a spontaneous dehydrogenation upon attachment to the electrode surface. This dehydrogenation is associated with a subsequent ionisation of the released hydrogen giving rise to a current that is associated with the adsorption of glucose, but not to its oxidation [37],[38],[61]. Once adsorbed, the glucose will be oxidised into gluconolactone which is then hydrolyzed into gluconic acid [37],[38],[61]. The adsorption resistance R_{ads} decreases in value until it reaches a minimum at a current density of around 12 µA cm^{-2}, before it increases again somewhat at higher current densities. The adsorption capacitance on the other hand,

C_{ads} , increases up to a current density of 12 µA cm^{-2}, before it levels out and seem to decrease at higher current densities. Both the observed effects on R_{ads} and C_{ads} may be related to a current dependent change in the adsorption rate of glucose in neutral PBS as suggested by [38, 61]. At the current density where glucose is expected to have reached the maximum coverage, the current has fallen to a level that is sustainable with the slowly generated glucose oxidation current only (adsorption max at 0.2 V vs RHE, or -0.42 V vs Ag|AgCl according to Vassilyev et al. [61]). Although the dehydrogenation of glucose (forming adsorbed gluconolactone intermediates) which is desorbed and hydrolyzed into gluconic acid, the adsorption energy and rate of adsorption of gluconic acid is noticeably lower than that of glucose [61]. Consequently, gluconic acid will by large escape the surface, hence not readsorb and be further oxidized, contributing negligible to the surface coverage and the overall current. Hence, the adsorbed gluconolactone formed during glucose dedhydrogenation and adsorption process on the Pt surface can be considered to be the dominating electroactive surface species. Furthermore, the voltammograms in Fig. 4. show a clear effect of adding glucose to the electrolyte with the appearance of new oxidation peaks (B, C and E). The small effects seen in the hydrogen UPD region suggests that glucose adsorbs to the electrode surface at these potentials but that the overall coverage is small compared to the adsorption / desorption of hydrogen (peak A and I) [38]. In addition, the adsorption of glucose may be influenced by adsorption of phosphate ions from the PBS solution, which somehow could reduce the number of active sites available for the electro-oxidation of glucose [37],[61],[62].
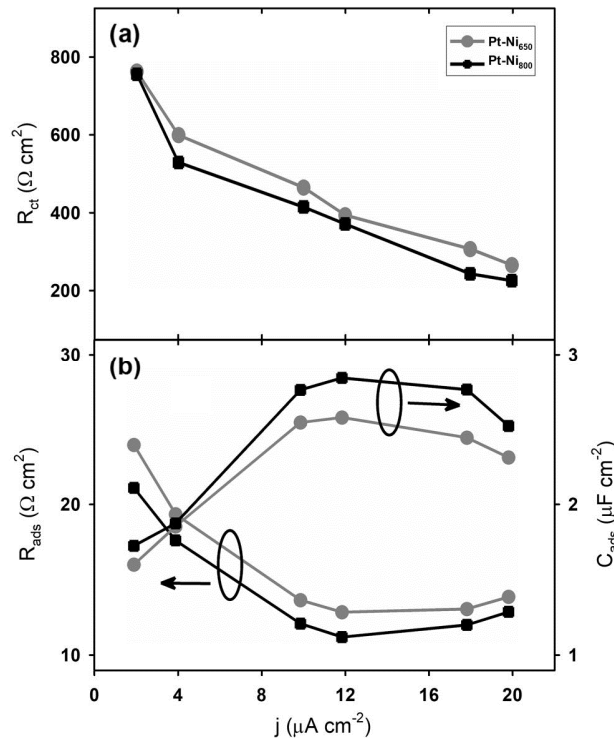

Figure 8: (a) The adsorption capacitance C_{ads} , and the adsorption resistance R_{ads} ; (b) The double layer capacitance C_{dl} and the charge transfer resistance R_{ct} of the Pt-Ni$_{650}$ and Pt-Ni$_{800}$ electrodes. All values measured as a function of load current density in deareated PBS with 5 mM glucose.

13

The charge transfer resistance R_{ct} can be viewed as the total charge transfer resistance of a multi-step reaction [36], and is consequently related to the overall rate of the glucose oxidation reaction at the surface of the catalyst layer. As expected for a Faradaic process, R_{ct} decreases with an increase in the load current density and subsequent increase in the glucose electro-oxidation rate [38, 61]. The values of the double layer capacitance, C_{dl}, are found to be 20.6 ± 2.8 and 20.5 ± 3.1 µF cm^{-2} for Pt-Ni$_{800}$ and Pt-Ni$_{650}$ electrodes, respectively. These are comparable with the values of the pure Pt electrode found in neutral and acid electrolytes [63-65].

The Tafel plots of the IR-corrected curves at 0 ppm DO are presented in Fig 9. The Tafel slopes and the exchange current density were extracted from the polarization curves in Fig. 5. One should bear in mind that a reliable determination of the Tafel slope will be limited due to the small range of current densities observed in the polarization curves. The slope of the Pt-Ni$_{800}$ electrodes (266 mV dec^{-1}) is comparable, yet higher than that of the Pt-Ni$_{650}$ electrodes (249 mV dec^{-1}). The exchange current density can be identified from the intercept of the tafelslope with the reversible potential for the glucose oxidation reaction. Since the nature of the reaction kinetics makes it difficult to determine the reversible potential, relative values for comparative analysis can be obtained by considering the intercept with the open circuit potential for the Pt-Ni$_{800}$ electrode. Hence, the apparent exchange current density of the Pt-Ni$_{800}$ electrodes (1.01 μA cm^{-2}) was found to be almost twice that of the Pt-Ni$_{650}$ electrodes (0.53 μA cm^{-2}). This result is in agreement with the improved performance observed for the Pt-Ni$_{800}$ electrodes (polarization curves, Fig 5) and in the R_{ads} and R_{ct} found from the EIS analysis in Fig 8, as well as the predicted enhancement of 2 times from section 3.2 which considers the effect of the roughness factor and identical *intrinsic* exchange current densities j_0 for both electrodes (hence what we are measuring in this case is in fact the *effective* exhange current density j_0*). Thus, considering the effective surface area (A_{eff}) based on the roughness factor (Eq.4), the apparent intrinsic exchange current density j_0 was calculated to 2.25 nA cm^{-2} for the Pt-Ni$_{650}$ and 2.05 nA cm^{-2} for the Pt-Ni$_{800}$ electrodes respectively. The assumption of an identical j_0 takes into consideration that the electrodes consist of the very same catalytic material, i.e. Pt and Ni. However, the intrinsic exchange current density is related to the properties of the actual catalytic site on the electrode surface, and some modifications could take place given the different annealing temperatures of 650 °C and 800 °C. Other effects may be the blocking of catalytic sites, and the amount of adsorption of reactive species on the catalyst surface.
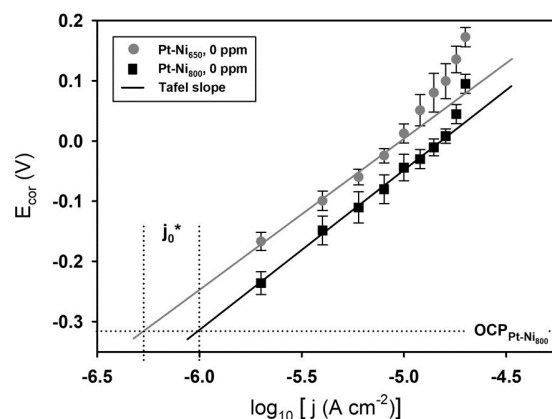
Figure 9: The Tafel plots of the Pt-Ni $_{650}$ and Pt-Ni $_{800}$ electrodes in deareated PBS solution with 5 mM glucose. The differences in the *effective* exchange current densities j_0* was found from the intercept of the slopes and the open circuit potential of the Pt-Ni $_{800}$ electrode.

The recorded exchange current density j_0 of the Pt-Ni alloy was found to be smaller than the exchange current density reported by Lam for a Pt-Co alloy (134 μ A cm^{-2}), under similar testing conditions (PBS, glucose concentration and DO level), whereas the Tafel slopes of the Pt-Ni alloy are approximately 1/2 of the Tafel slope of Pt-Co alloy (503 mV dec^{-1}) [66]. In contrast, the Tafel slopes of the Pt-Ni alloy in PBS were higher than that reported by Chen and Chen for the Pd-Ni/C alloy (approx. 192 mV dec^{-1}) in alkaline electrolytes [67].

3.4 Electrode stability

The chronopotentiometric responses of the Pt-Ni $_{800}$ and Pt-Ni $_{650}$ electrodes over a period of 72 hours at a constant load current density of 2 μA cm^{-2} in 10 mM PBS (containing 5 mM glucose) are presented in Fig. 10. The recording at *t = 0* shows the OCP just before the measurement onset.

During the first hour, the potentials of both electrodes increased due to the effect of the applied load current before the potentials were stabilized at approximately -0.18 V for the Pt-Ni $_{650}$ electrodes and -0.22 V for the Pt-Ni $_{800}$ electrodes (see insert in Fig. 10). The initial increase in electrode potential could be a result of the adsorption of glucose, its reaction intermediates and products as well as hydrogen and phosphate ions that slightly deactivates the surface until an equilibrium have been established, or it could be due to an initial reduction in active area. Although the potential drift rates of the Pt-Ni $_{650}$ and Pt-Ni $_{800}$ electrodes were initially estimated to be 110 mV h^{-1} and 180 mV h^{-1}, after the first hour respectively, this value reduced to 34 µV h^{-1} and 23 µV h^{-1}, respecitvely, during the last 4 hours. This shows the Pt-Ni electrodes stabilize under load with time in comparison to that of Pt-Zn electrodes (700 µV h^{-1} [27]). The Pt-Ni $_{800}$ electrodes have a slightly lower potential decay as compared to the Pt-Ni $_{650}$ electrodes.
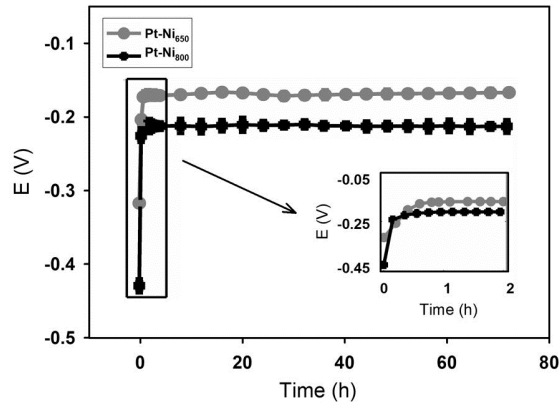
15

Figure 10: Chronopotentiometric response of the Pt-Ni$_{650}$ and Pt-Ni$_{800}$ electrodes at a load current density of 2 μA cm^{-2} in air saturated PBS with 5 mM glucose.

3   Conclusion

Microfabricated glucose selective anodes have been manufactured by annealing e-beam evaporated Pt and Ni thin films into a Pt-Ni alloy. The real surface area of the Pt-Ni$_{800}$ electrodes was found to be more than twice that of the Pt-Ni$_{650}$, which resulted in a lower adsorption resistance, R_{ads} (11.2 vs 12.8 Ω cm^2 at 12 µA cm^{-2}), a lower charge transfer resistance, R_{ct} (369.4 vs 390.6 Ω cm^2 at 12 µA cm^{-2}), a higher adsorption capacitance C_{ads} (2.85 vs 2.57 µF cm^{-2} at 12 µA cm^{-2}), a higher effective exchange current density j_0* (1.01 vs 0.53 µA cm^{-2}), and a lower area-specific ohmic resistance ASR_{ohm} (3.9 vs 4.1 Ω cm^2). These factors contributed in improving the overall glucose oxidation performance for the Pt-Ni$_{800}$ electrodes compared to the ones annealed at 650 °C. Still, the change in electrode potential of 0.1 V at 2 µA cm^{-2} in the presence of at 2 ppm DO suggests that any implementation in a mixed fuel environment should aim to reduce the amount of oxygen reaching the Pt-Ni anode surface. Future work will seek to combince this anode with an oxygen selective cathode in a combined micro fuel cell system running on endogenous fuel from the body.

Acknowledgements

References

1.	Larsson, B., et al., *Lessons from the first patient with an implanted pacemaker: 1958-2001*. PACE, 2003. **26**: p. 114-124.
2.	Grayson, A.C.R., et al., *A BioMEMS review: MEMS technology for physiologically integrated devices.* Proceedings of the IEEE, 2004. **92**(1): p. 6-21.
3.	Wise, K.D., et al., *Wireless implantable microsystems: high-density electronic interfaces to the nervous system.* Proceedings of the IEEE, 2004. **92**(1): p. 76-97.
4.	Desai, T.A., et al. *Implantation of microfabricated immunoisolating biocapsules*. 1998.
5.	Sbiaa, Z. *MEMS Fabricated Chip for an Implantable Drug Delivery Device*. in *2006 International Conference of the IEEE Engineering in Medicine and Biology Society*. 2006.
6.	Birchall, J. *Microfabricated microneedles for drug and gene delivery to skin*. in *2006 2nd IET Seminar on Micro/Nanotechnology in Medicine*. 2006.
7.	Grant, S.A., et al., *In vitro and in vivo measurements of ®ber optic and electrochemical sensors to monitor brain tissue pH.* Sensors and Actuators B: Chemical, 2001. **72**: p. 174-179.
8.	Ziaie, B. and K. Najafi, *An Implantable Microsystem for Tonometric Blood Pressure Measurement.* Biomedical Microdevices, 2001. **3**(4): p. 285-292.
9.	Krushinitskaya, O., et al. *Novel osmotic sensor for a continuous implantable blood-sugar reader*. in *6th International Workshop on Wearable, Micro, and Nano Technologies for Personalized Health (pHealth)*. 2009. Oslo, Norway: IEEE.
10.	Yang, Y., X.J. Wei, and J. Liu, *Suitability of a thermoelectric power generator for implantable medical electronic devices.* Journal of Physics D-Applied Physics, 2007. **40**(18): p. 5790-5800.
11.	Lay-Ekuakille, A., et al., *Thermoelectric generator design based on power from body heat for biomedical autonomous devices.* Medical Measurements and Applications, 2009. MeMeA 2009. IEEE International Workshop on, 2009: p. 1-4.
12.	Mitcheson, P.D., et al., *Energy Harvesting From Human and Machine Motion for Wireless Electronic Devices.* 2008. **96**(9): p. 1457-1486.
13.	Beeby, S.P., M.J. Tudor, and N.M. White, *Energy harvesting vibration sources for microsystems applications.* Measurement Science and Technology, 2006. **17**(12): p. R175.
14.	Nielsen, M.E., et al., *Sustainable energy from deep ocean cold seeps.* Energy \& Environmental Science, 2008. **1**(5): p. 584-593.
15.	Holmes, D.E., et al., *Microbial Communities Associated with Electrodes Harvesting Electricity from a Variety of Aquatic Sediments.* Microbial Ecology, 2004. **48**(2): p. 178-190.
16.	Ivanov, I., T. Vidakovic-Koch, and K. Sundmacher, *Recent Advances in Enzymatic Fuel Cells: Experiments and Modeling.* Energies, 2010. **3**(4): p. 803-846.
17.	Wang, H.-Y., et al., *Micro-sized microbial fuel cell: A mini-review.* Bioresource Technology, 2011. **102**(1): p. 235-243.
18.	Lovley, D.R., *Microbial fuel cells: novel microbial physiologies and engineering*

approaches. Current Opinion in Biotechnology, 2006: p. 327-332.

19. Kerzenmacher, S., et al., *Energy harvesting by implantable abiotically catalysed glucose fuel cells.* Journal of Power Sources, 2008. **182**: p. 1-17.

20. Kerzenmacher, S., et al., *A potentially implantable glucose fuel cell with Raney-platinum film electrodes for improved hydrolytic and oxidative stability.* Journal of Power Sources, 2011. **196**(3): p. 1264-1272.

21. Kerzenmacher, S., et al., *An abiotically catalyzed glucose fuel cell for powering medical implants: Reconstructed manufacturing protocol and analysis of performance.* Journal of Power Sources, 2008. **182**(1): p. 66-75.

22. Bagotzky, V.S. and Y.B. Vasilyev, *Some characteristics of oxidation reactions of organic compounds on platinum electrodes.* Electrochimica Acta, 1964. **9**(7): p. 869-882.

23. Brouzgou, A. and P. Tsiakaras, *Electrocatalysts for Glucose Electrooxidation Reaction: A Review.* Topics in Catalysis, 2015. **58**(18): p. 1311-1327.

24. Adzic, R.R., M.W. Hsiao, and E.B. Yeager, *Electrochemical oxidation of glucose on single crystal gold surfaces.* Journal of Electroanalytical Chemistry and Interfacial Electrochemistry, 1989. **260**(2): p. 475-485.

25. Brouzgou, A.a.P., A. and Tsiakaras, P., *PEMFCs and AEMFCs directly fed with ethanol: a current status comparative review.* Journal of Applied Electrochemistry, 2013. **43**(2): p. 119-136.

26. Parsons, R. and T. VanderNoot, *The oxidation of small organic molecules.* Journal of Electroanalytical Chemistry and Interfacial Electrochemistry, 1988. **257**(1): p. 9-45.

27. Kerzenmacher, S., et al., *Raney-platinum film electrodes for potentially implantable glucose fuel cells. Part 1: Nickel-free glucose oxidation anodes.* Journal of Power Sources, 2010. **195**(19): p. 6516-6523.

28. Gebhardt, U., J.R. Rao, and G.J. Richter, *A special type of raney-alloy catalyst used in compact biofuel cells.* Journal of Applied Electrochemistry, 1976. **6**(2): p. 127-134.

29. Oncescu, V. and D. Erickson, *A microfabricated low cost enzyme-free glucose fuel cell for powering low-power implantable devices.* Journal of Power Sources, 2011. **196**(22): p. 9169-9175.

30. Rapoport, B.I., J.T. Kedzierski, and R. Sarpeshkar, *A Glucose Fuel Cell for Implantable Brain–Machine Interfaces.* PLoS ONE, 2012. **7**(6): p. e38436.

31. Sree Harsha, K.S., *Principles of Vapor Deposition of Thin Films.* 1 ed. 2006, Oxford: Elsevier Science. 1176.

32. Do, U.P., et al., *Thin film nanoporous electrodes for the selective catalysis of oxygen in abiotically catalysed micro glucose fuel cells.* Journal of Materials Science, 2016. **51**(19): p. 9095-9107.

33. Lukaszewski, M., M. Soszko, and A. Czerwinski, *Electrochemical Methods of Real Surface Area Determination of Noble Metal Electrodes - an Overview.* International Journal of Electrochemical Science, 2016. **11**(6): p. 4442-4469.

34. Rudi, S., et al., *Comparative Study of the Electrocatalytically Active Surface Areas (ECSAs) of Pt Alloy Nanoparticles Evaluated by H-upd and CO-stripping voltammetry.* Electrocatalysis, 2014. **5**(4): p. 408-418.

35. Trasatti, S. and O.A. Petrii, *Real surface area measurements in electrochemistry.* Journal

of Electroanalytical Chemistry, 1992. **327**(1): p. 353-376.

36. Doyle, R.L., et al., *Non-Enzymatic Glucose Oxidation at Electrocatalytic Metal Oxide Films* ECS Transactions, 2013. **53**(16): p. 1-15.

37. Pasta, M., et al., *Optimizing operating conditions and electrochemical characterization of glucose–gluconate alkaline fuel cells.* Journal of Power Sources, 2011. **196**(3): p. 1273-1278.

38. Ernst, S., J. Heitbaum, and C.H. Hamann, *The electrooxidation of glucose in phosphate buffer solutions: Part I. Reactivity and kinetics below 350 mV/RHE.* Journal of Electroanalytical Chemistry and Interfacial Electrochemistry, 1979. **100**(1): p. 173-183.

39. Bevington, P.R. and D.K. Robinson, *Data Reduction and Error Analysis for the Physical Sciences*. 3rd ed. 1969: McGraw Hill, New York.

40. Brug, G.J., et al., *The analysis of electrode impedances complicated by the presence of a constant phase element.* Journal of Electroanalytical Chemistry and Interfacial Electrochemistry, 1984. **176**(1): p. 275-295.

41. Sreemany, M. and S. Sen, *Effect of substrate temperature and annealing temperature on the structural, electrical and microstructural properties of thin Pt films by rf magnetron sputtering.* Applied Surface Science, 2006. **253**(5): p. 2739-2746.

42. Derkach, V., et al., *Grain boundary migration and grooving in thin 3-D systems.* Acta Materialia, 2014. **65** p. 194–206.

43. Génin, F.Y., W.W. Mullins, and P. Wynblatt, *The effect of stress on grain boundary grooving.* Acta Metallurgica et Materialia, 1993. **41**(12): p. 3541-3547.

44. Morrison, A.R.T., S.S. Hosseiny, and R. Wüthrich, *Platinum-like oxidation of nickel surfaces by rapidly switching voltage to generate highly active bifunctional catalysts.* Electrochemistry Communications, 2016. **67**: p. 22-25.

45. Fu, T.R., et al., *Total hemispherical radiation properties of oxidized nickel at high temperatures.* Corrosion Science, 2014. **83**: p. 272-280.

46. Hudak, E.M., J.T. Mortimer, and H.B. Martin, *Platinum for neural stimulation: voltammetry considerations.* Journal of Neural Engineering, 2010. **7**(2): p. 026005.

47. Cogan, S.F., *Neural Stimulation and Recording Electrodes.* Annual Review of Biomedical Engineering, 2008. **10**(1): p. 275-309.

48. Robblee, L.S. and T.L. Rose, *The electrochemistry of electrical stimulation.* Ann. Int. Conf. IEEE Eng. Med. Biol. Soc., 1990. **12**: p. 1479.

49. Alsabet, M., M. Grden, and G. Jerkiewicz, *Electrochemical Growth of Surface Oxides on Nickel. Part 3: Formation of beta-NiOOH in Relation to the Polarization Potential, Polarization Time, and Temperature.* Electrocatalysis, 2015. **6**(1): p. 60-71.

50. Mahshid, S.S., et al., *Template-based electrodeposition of Pt/Ni nanowires and its catalytic activity towards glucose oxidation.* Electrochimica Acta, 2011. **58**: p. 551-555.

51. Mahshid, S.S., et al., *Preparation of Pulse Deposited Pt/Ni Nanowires Electrode for Glucose Detection in Alkaline Solution.* International Journal of Theoretical and Applied Nanotechnology (IJTAN), 2012. **1**(1): p. 66-72.

52. Beverskog, B. and I. Puigdomenech, *Revised Pourbaix diagrams for nickel at 25–300 °C.* Corrosion Science, 1997. **39**(5): p. 969-980.

53. Bolzan, A.E., T. Iwasita, and W. Vielstich, *On the Electrochemical Oxidation of Glucose:*

Identification of Volatile Products by On-Line Mass Spectroscopy. Journal of The Electrochemical Society, 1987. **134**(12): p. 3052-3058.

54. Rao, J.R., et al., *The performance of glucose electrodes and the characteristics of different biofuel cell constructions.* Bioelectrochemistry and Bioenergetics, 1976. **3**(1): p. 139-150.

55. Ernst, S., J. Heitbaum, and C.H. Hamann, *The Electrooxidation of Glucose in Phosphate Buffer Solutions: Kintetics and Reaction Mechanism.* Berichte der Bunsengesellschaft für physikalische Chemie, 1980. **84**(1): p. 50-55.

56. de Mele, M.F.L., H.A. Videla, and A.J. Arvia, *Potentiodynamic Study of Glucose Electro-Oxidation at Bright Platinum Electrodes.* Journal of The Electrochemical Society, 1982. **129**: p. 2207-2213.

57. Yan, X., X. Ge, and S. Cui, *Pt-decorated nanoporous gold for glucose electrooxidation in neutral and alkaline solutions.* Nanoscale Research Letters, 2011. **6**(1): p. 1-6.

58. Becerik, I., F. Ficicioglu, and F. Kadirgan, *Effect of Temperature on the Electrochemical Oxidation of Some Organic Molecules on Pt Doped Conducting Polymer Coated Electrodes.* TURKISH JOURNAL OF CHEMISTRY, 1999. **23**: p. 353/360.

59. Habrioux, A., et al., *Activity of Platinum–Gold Alloys for Glucose Electrooxidation in Biofuel Cells.* The Journal of Physical Chemistry B, 2007. **111**(34): p. 10329-10333.

60. ZAHNER, *Thales manual*, in *Thales 04: SIM - Simulation and Fitting*. 2013.

61. Vassilyev, Y.B., O.A. Khazova, and N.N. Nikolaeva, *Kinetics and mechanism of glucose electrooxidation on different electrode-catalysts: Part I. Adsorption and oxidation on platinum.* Journal of Electroanalytical Chemistry and Interfacial Electrochemistry, 1985. **196**(1): p. 105-125.

62. de Mele, M.F.L., H.A. Videla, and A.J. Arvía, *The electrooxidation of glucose on platinum electrodes in buffered media.* Bioelectrochemistry and Bioenergetics, 1983. **10**(2): p. 239-249.

63. Pajkossy, T. and D.M. Kolb, *Double layer capacitance of Pt(111) single crystal electrodes.* Electrochimica Acta, 2001. **46**(20): p. 3063-3071.

64. Pell, W.G., A. Zolfaghari, and B.E. Conway, *Capacitance of the double-layer at polycrystalline Pt electrodes bearing a surface-oxide film.* Journal of Electroanalytical Chemistry, 2002. **532**(1): p. 13-23.

65. Rosen, M., D.R. Flinn, and S. Schuldiner, *Double Layer Capacitance on Platinum in 1 M H 2 SO 4 from the Reversible Hydrogen Potential to the Oxygen Formation Region.* Journal of The Electrochemical Society, 1969. **116**(8): p. 1112-1116.

66. Lam, C.M., *Glucose oxidation on different electrocatalysis: Mechanism and sensor applications*. 2000, The University of Hong Kong: Hong Kong.

67. Chen, C.-C. and L.-C. Chen, *Synthesis and characterization of Pd-Ni core-shell nanocatalysts for alkaline glucose electrooxidation.* RSC Adv., 2015. **5**: p. 53333-53339.